Acta Crystallographica Section F
Structural Biology and Crystallization Communications
ISSN 1744-3091

Crystallization and preliminary X-ray crystallographic analysis of human Apaf-1-interacting protein

Wonchull Kang and Jin Kuk Yang*

Department of Chemistry, College of Natural Sciences, Soongsil University, Seoul 156-743, Republic of Korea

Correspondence e-mail: jinkukyang@ssu.ac.kr

Received 16 August 2012
Accepted 13 October 2012

Apaf-1-interacting protein (APIP) is known to inhibit two different types of cell death: caspase-1-dependent pyroptosis and caspase-9-dependent apoptosis. APIP is also involved in the methionine-salvage pathway, where it is called 5-methylthioribulose-1-phosphate dehydratase (MtnB). The enzyme activity seems to be essential for inhibition of pyroptosis by APIP, but not for inhibition of apoptosis. In this study, human APIP was overproduced in *Escherichia coli*, purified and crystallized. An X-ray diffraction data set was collected to 2.40 Å resolution and the crystals belonged to space group $C222_1$, with unit-cell parameters $a = 106.61$, $b = 107.50$, $c = 189.76$ Å. Given that four APIP molecules exist in the asymmetric unit, the Matthews coefficient is 2.70 Å^3 Da^{-1} and the corresponding solvent content is 54.4%.

1. Introduction

Apaf-1-interacting protein (APIP) has been shown to inhibit at least two types of cell death: caspase-9-dependent apoptosis and caspase-1-dependent pyroptosis (Cho *et al.*, 2004, 2007; Ko *et al.*, 2012). Firstly, APIP inhibits activation of caspase-9 in the mitochondrial apoptosis pathway. It seems that APIP exerts this function in both Apaf-1-dependent and Apaf-1-independent ways. APIP was initially identified as an Apaf-1-binding protein from a yeast two-hybrid assay and was thus named (Cho *et al.*, 2004). APIP binds Apaf-1 at the caspase-recruiting domain (CARD) in competition with caspase-9 and thereby inhibits the activation of caspase-9 in the mitochondrial apoptosis pathway (Cho *et al.*, 2004). In addition, APIP also inactivates caspase-9 in an Apaf-1-independent manner. APIP induces the sustained activation of AKT and ERK1/2, which inactivate caspase-9 through direct phosphorylation (Cho *et al.*, 2007). However, it has not yet been characterized how APIP becomes involved in kinase signalling pathways and exerts its kinase-activating function. Secondly, APIP inhibits the pro-inflammatory cell death known as pyroptosis involving caspase-1 activation. This function of APIP has very recently been revealed from functional genetic screening of the single-nucleotide polymorphism (SNP) regulating pyroptosis induced by bacterial infection (Ko *et al.*, 2012). One intergenic SNP that reduces *APIP* expression was associated with increased caspase-1-mediated cell death in response to *Salmonella*. Experiments altering the *APIP* expression level showed that APIP inhibits caspase-1-dependent pyroptosis and also caspase-9-dependent apoptosis (Ko *et al.*, 2012).

Regarding the mechanism of APIP inhibition of cell death, a link to its enzymatic activity has been shown in the case of caspase-1-dependent pyroptosis. Based on sequence similarity, APIP is annotated in UniProtKB (http://www.uniprot.org) as an enzyme of the methionine-salvage pathway called 5-methylthioribulose-1-phosphate dehydratase (MtnB). Very interestingly, the enzymatic activity of APIP was shown to be essential for pyroptosis but not for caspase-9-dependent apoptosis (Ko *et al.*, 2012). APIP seems to inhibit caspase-9 cell death by other mechanisms that are irrelevant to the enzyme activity, *i.e.* by binding to the CARD region of Apaf-1 in competition with caspase-9 or by somehow activating AKT and ERK1/2.

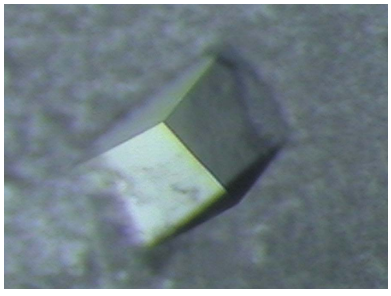

In the hope of acquiring clues to the molecular mechanism of APIP, we initiated its crystallographic analysis in order to elucidate its structural details. Here, we report its crystallization and X-ray data collection as an initial step in structural analysis.

2. Experimental procedures

2.1. Cloning

The gene region for residues 20–242 of human APIP was amplified by polymerase chain reaction from its cDNA (a gift from Dr Y.-K. Jung of Seoul National University, Republic of Korea). The amplified gene was digested with the restriction enzymes *Nde*I and *Xho*I (New England Biolabs, USA) and ligated into pET21a (Novagen, USA). The nucleotide sequences were confirmed by sequencing (Bionics, Republic of Korea).

2.2. Protein overproduction and purification

Escherichia coli strain Rosetta 2(DE3) was transformed with the expression vector constructed as above and cultured with shaking at 310 K in Luria–Bertani medium containing 50 µg ml^{-1} ampicillin. When the OD_{600} reached 0.6, the culture was cooled to 293 K and protein overproduction was induced by the addition of isopropyl β-D-1-thiogalactopyranoside (IPTG) to a final concentration of 0.5 m*M*. The cells were cultured at 293 K for an additional 16 h after IPTG induction and were harvested by centrifugation at 5000 rev min^{-1} (4416*g*) for 30 min (Hanil Supra 22K with rotor 11, Republic of Korea).

The harvested cells were resuspended in working buffer [20 m*M* Tris–HCl, 5%(*v*/*v*) glycerol, 0.1 m*M* TCEP, 100 m*M* sodium chloride pH 8.0] containing 10 m*M* imidazole and 0.1 m*M* phenylmethylsulfonyl fluoride. The resuspended cells were lysed by sonication with a VCX500 ultrasonic processor (Sonics & Materials, USA) and the cell lysate was centrifuged at 15 000 rev min^{-1} for 60 min (Hanil Supra 22K with rotor 7, Republic of Korea). The supernatant was filtered through a membrane filter with 0.45 µm pore size (Advantec, Japan) and applied onto a HisTrap column (GE Healthcare Biosciences, USA). The bound protein was eluted with a 0–0.5 *M* imidazole gradient and the eluted sample (at 0.2–0.3 *M* imidazole) was passed through a HiPrep Desalting column (GE Healthcare Biosciences, USA) to removal the imidazole. Next, a HiTrap Q Sepharose FF anion-exchange column (GE Healthcare Biosciences, USA) was applied with a linear gradient of 0–1.0 *M* NaCl; APIP eluted at about 0.4 *M* NaCl. The pooled sample was further purified by size-exclusion chromatography (Superdex 200; GE Healthcare Biosciences, USA). The final purified sample was concentrated to 15 mg ml^{-1} by centrifugal ultrafiltration (Amicon Ultra, Millipore, USA). The purity of the protein was judged by SDS–PAGE and the concentration was determined by measuring the absorbance at 280 nm using a calculated extinction coefficient of 1.26 mg^{-1} ml cm^{-1} (http://www.expasy.org). The final purified and concentrated sample also contained 20 m*M* Tris–HCl, 5%(*v*/*v*) glycerol, 0.1 m*M* TCEP, 100 m*M* sodium chloride at pH 8.0.

2.3. Crystallization and X-ray data collection

Crystallization conditions were initially searched for by the hanging-drop vapour-diffusion method using commercial screening kits from Hampton Research, Emerald BioSystems and Qiagen. The hanging drop was prepared by mixing 1.0 µl protein sample and an equal volume of reservoir solution and was equilibrated against 200 µl reservoir solution. Refinement of the reservoir solution composition from a hit from the initial screening was carried out by varying the concentrations of the ingredients. The final optimized composition was 0.04 *M* citric acid, 0.06 *M* bis-tris propane, 5%(*v*/*v*) glycerol, 18–21%(*w*/*v*) polyethylene glycol (PEG) 3350. Crystals appeared within 5 d at 295 K and reached their maximum dimensions after two weeks, with typical dimensions of 0.2 × 0.2 × 0.2 mm.

For cryoprotection, the concentrations of glycerol and PEG 3350 in the hanging drop were continuously increased by equilibration of the drop against a cryoprotecting solution with 25%(*w*/*v*) PEG 3350 and 10%(*v*/*v*) glycerol for 2–3 d. The crystal was then taken from the drop and directly flash-cooled in liquid nitrogen before data collection.

X-ray diffraction data were collected at 100 K using an ADSC Quantum 270 CCD detector on synchrotron beamline 7A at Pohang Accelerator Laboratory, Republic of Korea. 360 images were collected for the full data set and each image was recorded with an exposure of 3 s and 1° oscillation. Intensity data were processed, merged and scaled with *MOSFLM* and *SCALA* from the *CCP*4 program suite (Winn *et al.*, 2011).

3. Results and discussion

Human APIP (residues 20–242) was overproduced in *E. coli* and purified by column chromatography. The purified protein was concentrated to 15 mg ml^{-1} for crystallization trials. Small cube-shaped crystals grew in 5 d from condition No. 39 of PEG/Ion 2 (Hampton Research), which consists of 0.04 *M* citric acid, 0.06 *M* bis-tris propane, 20%(*w*/*v*) polyethylene glycol 3350 (final pH 6.4). Subsequent trials revealed that the largest crystals could be reproduced well using reservoir solution consisting of 0.04 *M* citric acid, 0.06 *M* bis-tris propane, 5%(*v*/*v*) glycerol, 18–21%(*w*/*v*) PEG 3350 (final pH 6.4). The crystals reached maximum dimensions of 0.2 × 0.2 × 0.2 mm two weeks after setup (Fig. 1).

The crystals were easily damaged during transfer into the cryoprotecting solution, which had a composition of 0.04 *M* citric acid, 0.06 *M* bis-tris propane, 10%(*v*/*v*) glycerol, 25%(*w*/*v*) PEG 3350 (final pH 6.4). Therefore, a slow and continuous increase in the glycerol and PEG 3350 concentrations was attempted before flash-cooling. We added 2.0 µl reservoir solution to a drop containing fully grown crystals and equilibrated it against a cryoprotecting solution with higher concentrations of glycerol and PEG 3350: 10%(*v*/*v*) and 25%(*w*/*v*), respectively. After equilibration for 2–3 d, the crystal was flash-cooled in liquid nitrogen and subjected to data collection. Using

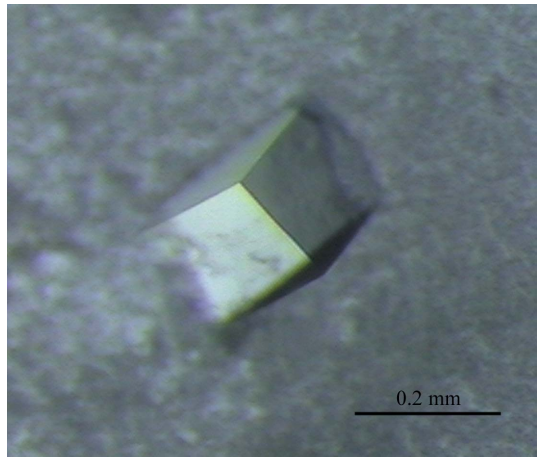

Figure 1
Cube-shaped crystal of APIP.

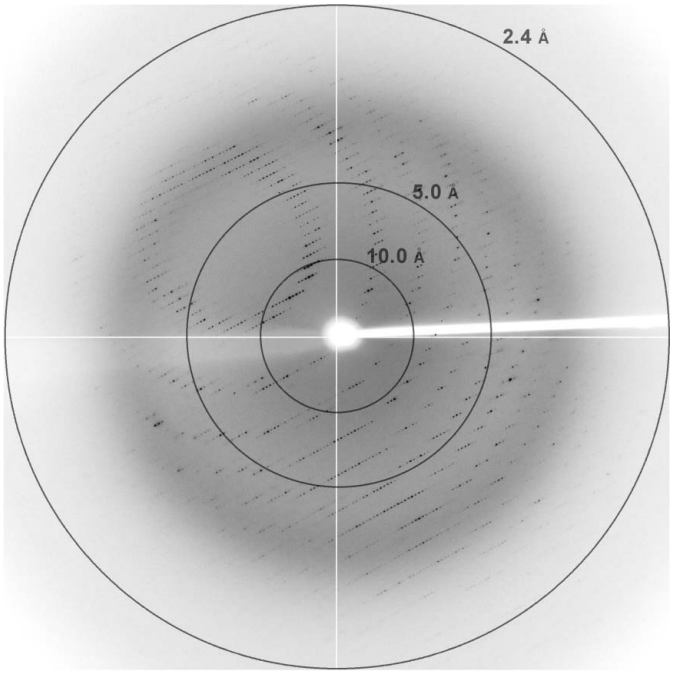

Figure 2
Representative diffraction image obtained on beamline 7A of Pohang Accelerator Laboratory, Republic of Korea. The crystal-to-detector distance was 300 mm and the wavelength was 0.9999 Å.

this procedure, well defined diffraction spots were observed in the images, indicating minimal crystal damage (Fig. 2). The crystals diffracted to 2.40 Å resolution on beamline 7A of Pohang Accelerator Laboratory. The crystals belonged to the *C*-centred orthorhombic system, with unit-cell parameters a = 106.61, b = 107.50, c = 189.76 Å. Systematic extinctions unambiguously indicated $C222_1$ as the space group. The diffraction data set consisted of 42 964 unique reflections and was 99.9% complete, with a multiplicity of 14.1 and an $R_{\rm merge}$ of 9.8%. Table 1 summarizes the statistics of the data collection. Given that four APIP molecules are present in the asymmetric unit, the Matthews coefficient was 2.70 Å^3 Da^{-1} and the corresponding solvent content was 54.4%. A *BLAST* search against the Protein Data Bank showed that an MtnB enzyme structure has not yet been reported; the most similar protein structures were the FucA enzymes from *Aquifex aeolicus* (PDB entry 2irp; RIKEN Structural Genomics/Proteomics Initiative, unpublished work) and *Thermus thermophilus* (PDB entry 2fk5; Jeyakanthan *et al.*, 2005), which showed 26% and 23% sequence identity over 194 and 196 aligned residues, respectively. Molecular-replacement calculations with the FucA structures as search models were not successful; the multi-wavelength anomalous diffraction method is therefore now being attempted for structure solution.

Table 1
Summary of data-collection statistics.

Values in parentheses are for the highest resolution shell.

Space group	$C222_1$
Unit-cell parameters (Å)	a = 106.61, b = 107.50, c = 189.76
Resolution (Å)	30.00–2.40 (2.52–2.40)
No. of measured reflections	2046359
No. of unique reflections	42964
$R_{\rm merge}$† (%)	9.8 (37.7)
Completeness (%)	99.9 (100.0)
$\langle I/\sigma(I)\rangle$	6.8 (2.0)
Multiplicity	14.1 (14.6)

† $R_{\rm merge} = \sum_{hkl}\sum_i |I_i(hkl) - \langle I(hkl)\rangle| / \sum_{hkl}\sum_i I_i(hkl)$, where $I(hkl)$ is the intensity of reflection hkl, $\sum_{hkl}$ is the sum over all reflections and $\sum_i$ is the sum over i measurements of reflection hkl.

This research was supported by the Basic Science Research Program through the National Research Foundation of Korea (NRF) funded by the Ministry of Education, Science and Technology (2009-0074396) and was also supported by a grant from the Korea Healthcare Technology R&D Project, Ministry of Health and Welfare, Republic of Korea (A092006). The authors thank H. M. Lee for earlier work on this project and the staff of beamline 7A at Pohang Accelerator Laboratory for help with data collection.

References

Cho, D.-H., Hong, Y.-M., Lee, H.-J., Woo, H.-N., Pyo, J.-O., Mak, T. W. & Jung, Y.-K. (2004). *J. Biol. Chem.* **279**, 39942–39950.
Cho, D.-H., Lee, H.-J., Kim, H.-J., Hong, S.-H., Pyo, J.-O., Cho, C. & Jung, Y.-K. (2007). *Oncogene*, **26**, 2809–2814.
Jeyakanthan, J., Taka, J., Kikuchi, A., Kuroishi, C., Yutani, K. & Shiro, Y. (2005). *Acta Cryst.* F**61**, 1075–1077.
Ko, D. C., Gamazon, E. R., Shukla, K. P., Pfuetzner, R. A., Whittington, D., Holden, T. D., Brittnacher, M. J., Fong, C., Radey, M., Ogohara, C., Stark, A. L., Akey, J. M., Dolan, M. E., Wurfel, M. M. & Miller, S. I. (2012). *Proc. Natl. Acad. Sci. USA*, **109**, E2343–E2352.
Winn, M. D. *et al.* (2011). *Acta Cryst.* D**67**, 235–242.